

# Effects of next-nearest-neighbor hopping $t'$ on the electronic structure of cuprates

K. Tanaka, T. Yoshida, A. Fujimori, D.H. Lu<sup>†</sup>, Z.-X. Shen<sup>†</sup>, X.-J. Zhou<sup>†\*</sup>, H. Eisaki<sup>†</sup>,  
Z. Hussain<sup>\*</sup>, S. Uchida, Y. Aiura<sup>‡</sup>, K. Ono<sup>‡</sup>, T. Sugaya<sup>‡</sup>, T. Mizuno<sup>‡</sup>, and I. Terasaki<sup>‡</sup>

*Department of Physics and Department of Complexity Science and Engineering, University of Tokyo, Tokyo, 113-0033, Japan*

<sup>†</sup>*Department of Applied Physics and Stanford Synchrotron Radiation  
Laboratory, Stanford University, Stanford, CA 94305, USA*

<sup>\*</sup>*Advanced Light Source, Lawrence Berkely National Lab, Berkeley, CA 94720, USA*

<sup>‡</sup>*National Institute for Advanced Industrial Science and Technology (AIST), Tsukuba, 305-8568, Japan*

<sup>‡</sup>*Photon Factory, IMSS, High Energy Accelerator Research Organization, Tsukuba, 305-0801, Japan*

<sup>‡</sup>*Department of Applied Physics, Waseda University, Tokyo 169-8555, Japan*

(Dated: November 16, 2018)

Photoemission spectra of underdoped and lightly-doped  $\text{Bi}_{2-z}\text{Pb}_z\text{Sr}_2\text{Ca}_{1-x}\text{R}_x\text{Cu}_2\text{O}_{8+y}$  ( $R = \text{Pr, Er}$ ) (BSCCO) have been measured and compared with those of  $\text{La}_{2-x}\text{Sr}_x\text{CuO}_4$  (LSCO). The lower-Hubbard band of the insulating BSCCO, like  $\text{Ca}_2\text{CuO}_2\text{Cl}_2$ , shows a stronger dispersion than  $\text{La}_2\text{CuO}_4$  from  $\mathbf{k} \sim (\pi/2, \pi/2)$  to  $\sim (\pi, 0)$ . The flat band at  $\mathbf{k} \sim (\pi, 0)$  is found generally deeper in BSCCO. These observations together with the Fermi-surface shapes and the chemical potential shifts indicate that the next-nearest-neighbor hopping  $|t'|$  of the single-band model is larger in BSCCO than in LSCO and that  $|t'|$  rather than the super-exchange  $J$  influences the pseudogap energy scale.

PACS numbers: 74.72.Hs, 79.60.-i, 71.28.+d

Since the discovery of the high-temperature superconductivity in  $\text{La}_{2-x}\text{Ba}_x\text{CuO}_4$ , many families of high- $T_c$  cuprates have been synthesized. Common features are that they have the two-dimensional  $\text{CuO}_2$  planes and a similar phase diagram as a function of hole doping. This has naturally lead most of studies to emphasize the common features of the cuprate electronic structures rather than emphasizing differences among them. On the other hand, there are differences among the different families of cuprates such as the significant variation in the magnitude of the superconducting gap and the critical temperature ( $T_c$ ) at optimal doping,  $T_{c,\text{max}}$ . A systematic investigation of the differences between the different families of cuprates may enable us to understand the origin of the different  $T_{c,\text{max}}$ 's and eventually the mechanism of superconductivity. So far, some studies have focused on the material dependence from empirical points of view. In an early work, Ohta *et al.* [1] proposed the differences in the position of the apical oxygen and the resulting differences in the Madelung potentials as the origin of the different  $T_{c,\text{max}}$ 's. Feiner *et al.* [2] proposed that the  $p_z$  orbital of the apical oxygen hybridizing with the  $d_{3z^2-r^2}$  orbital of Cu and the  $p_{x,y}$  orbitals of the in-plane oxygen affects the next-nearest-neighbor hopping parameter  $t'$  in the single-band model description of the  $\text{CuO}_2$  plane, and thereby  $T_{c,\text{max}}$  in the context of the van Hove singularity scenario [3]. Those differences between the cuprate families may affect the stability of the Zhang-Rice singlet [1], instability toward charge stripes [4] and so on, and hence  $T_{c,\text{max}}$ . Recently, Pavarini *et al.* [5] have demonstrated the correlation between  $t'$  (of the bonding band for multilayer cuprates) and  $T_{c,\text{max}}$  from their tight-binding model analysis of the first-principles band structures of numerous high- $T_c$  cuprates. For the differences in  $T_{c,\text{max}}$ , the various degrees of disorder has also been considered im-

portant [6].

In the present work, on the basis of photoemission data, we focus on differences in the electronic structure of the cuprates such as the band dispersion of the parent insulator and the doped compounds as well as the Fermi surface shape between  $\text{La}_{2-x}\text{Sr}_x\text{CuO}_4$  (LSCO) and  $\text{Bi}_2\text{Sr}_2\text{CaCu}_2\text{O}_{8+\delta}$  (BSCCO). We have found that lightly-doped and underdoped BSCCO show a stronger band dispersion along the “underlying Fermi surface” than its counter part in LSCO. Given that  $J$  does not change much between the two families ( $J_{\text{LSCO}} \sim 139$  meV and  $J_{\text{BSCCO}} \sim 127$  meV from two-magnon Raman scattering [7, 8, 9] and magnetic neutron scattering [10]), we attribute the observed differences to the variation in  $t'$ , a finding consistent with the band structure estimates of  $t'$  [5] and the  $t$ - $J$  model calculation on the impact of  $t'$  on the electronic structure around  $\mathbf{k} \sim (\pi, 0)$  [11].

So far, photoemission studies of LSCO have covered a wide composition range from the lightly-doped to overdoped regions and systematic data are available for the evolution of the pseudogap [12], Fermi surface [13, 14, 15], band dispersion [14, 16] and chemical potential shift [17]. Although BSCCO has been extensively studied by angle-resolved photoemission spectroscopy (ARPES) owing to its stable cleavage surfaces in an ultra high vacuum, the available range of hole concentration has been largely limited to  $\delta = 0.10$ - $0.17$ . Recently, high quality single crystals of heavily underdoped BSCCO were synthesized by rare-earth ( $R$ ) substitution for Ca and the doping dependence of thermodynamic and transport properties have been systematically studied [18, 19, 20]. The present study was made possible by the availability of such deeply underdoped BSCCO samples.

Single crystals of  $\text{Bi}_{1.2}\text{Pb}_{0.8}\text{Sr}_2\text{ErCu}_2\text{O}_8$  and  $\text{Bi}_2\text{Sr}_2\text{Ca}_{1-x}\text{R}_x\text{Cu}_2\text{O}_{8+y}$  ( $R = \text{Pr, Er}$ ) were grown

TABLE I: Chemical compositions, hole concentration  $\delta$  and  $T_c$  of BSCCO samples studied in the present work.

$\text{Bi}_2\text{Sr}_2\text{Ca}_{1-x}\text{R}_x\text{Cu}_2\text{O}_8$	$\delta$	$T_c$ (K)
$R = \text{Er}, x = 1$	0.025	-
$R = \text{Er}, x = 0.5$	0.05	-
$R = \text{Er}, x = 0.1$	0.135	87
$R = \text{Pr}, x = 0.43$	0.1	48
$R = \text{Pr}, x = 0.25$	0.135	88
$R = \text{Pr}, x = 0.1$	0.17	86
$\text{Bi}_{1.2}\text{Pb}_{0.8}\text{Sr}_2\text{ErCu}_2\text{O}_8$	0.04	-

by the self-flux method. X-ray diffraction showed no trace of impurity phases. Details of the sample preparation are given elsewhere [19, 20]. The hole concentration  $\delta$  per Cu atom was determined using the empirical relationship between  $\delta$  and the room-temperature thermopower [21]. The  $\delta$  and  $T_c$  of the measured samples are listed in Table. 1. The  $x = 0.5$  and 1.0 Er samples are antiferromagnetic (AF) insulators. The Laue patterns of the Pb doped samples showed no superlattice modulation of the Bi-O layers, which eliminated superstructure signals in ARPES spectra. Single crystals of LSCO were grown by the traveling-solvent floating-zone method. The  $T_c$  of  $x = 0.07, 0.10, 0.15$  and  $0.22$  samples were 14, 29, 41 and 20 K, respectively, and  $x = 0.00, 0.03$  samples were non-superconducting [16].

ARPES measurements of BSCCO were carried out at beamline 5-4 of Stanford Synchrotron Radiation Laboratory (SSRL). Incident photons had an energy of  $h\nu = 19$  eV. A SCIENTA SES-200 analyzer was used in the angle mode with the total energy and momentum resolutions of  $\sim 14$  meV and  $\sim 0.25^\circ$ , respectively. Samples were cleaved *in situ* under an ultrahigh vacuum of  $10^{-11}$  Torr, and were cooled down to  $\sim 10$  K. The position of the Fermi level ( $E_F$ ) was calibrated with gold spectra. ARPES measurements with  $h\nu = 30-60$  eV at 85 K were performed at beamline BL-1C of Photon Factory (PF) using an ARUPS-10 analyzer. The overall energy resolution varied from 130 to 150 meV. ARPES measurements of LSCO were carried out at BL10.0.1.1 of Advanced Light Source (ALS), using incident photons of 55.5 eV at 20 K as described elsewhere [16]. Angle-integrated photoemission spectroscopy (AIPES) measurements of BSCCO samples were carried out using the He I resonance line ( $h\nu = 21.2$  eV) with an OMICRON 125EA analyzer. The samples were cleaved *in situ* and measured at  $\sim 7$  K with the energy resolution of  $\sim 25$  meV.

Figure 1 shows the ARPES spectra of insulating  $\text{Bi}_{1.2}\text{Pb}_{0.8}\text{Sr}_2\text{ErCu}_2\text{O}_8$  ( $\delta \sim 0.04$ ) along the diagonal  $(0,0)-(\pi,\pi)$  direction in the second Brillouin zone (BZ). The figure shows a single dispersive feature corresponding to the lower Hubbard band, which moves closest to  $E_F$  at  $\sim(\pi/2, \pi/2)$ . There is no sharp peak crossing

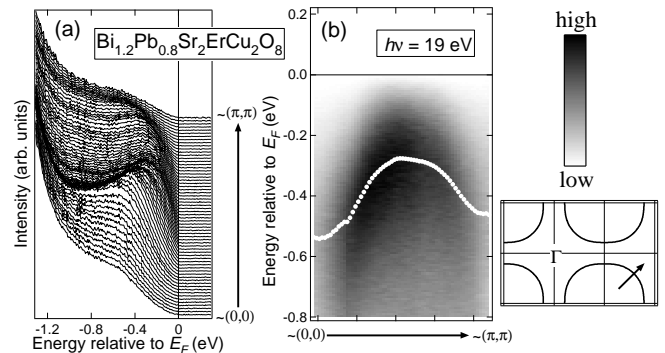


FIG. 1: ARPES spectra of insulating  $\text{Bi}_{1.2}\text{Pb}_{0.8}\text{Sr}_2\text{ErCu}_2\text{O}_8$  along the  $(0,0)-(\pi,\pi)$  direction. (a) EDC's, (b) Intensity plot in the  $E-k$  plane. The white circles indicate the energy of the maximum curvature in the EDC's.

$E_F$ . This is contrasted with LSCO of similar doping level where a tiny but sharp peak crosses  $E_F$  [16], and is consistent with the insulating behavior of the present compound [20]. (Note that LSCO with  $x \sim 0.03$  shows metallic behaviour at  $T > 100$  K.)

Figure 2 shows ARPES spectra along the “underlying Fermi surface” [22]. One can again see a single dispersive feature between  $-0.6$  and  $-0.2$  eV, as in case of  $\text{Ca}_2\text{CuO}_2\text{Cl}_2$  (CCOC) and  $\text{Sr}_2\text{CuO}_2\text{Cl}_2$  [11, 22, 23]. In Fig. 2(c), we have plotted the peak position of the spectra marked in Fig. 2(a) referenced to the binding energy of the peak at  $(\pi/2, \pi/2)$  against  $|\cos k_x a - \cos k_y a|/2$ . The nearly straight line shows approximately  $d_{x^2-y^2}$ -like gap anisotropy on the underlying Fermi surface [24]. Combining Figs. 1(b) and 2(b), one can conclude that the band dispersion in the insulating BSCCO is nearly isotropic around  $(\pi/2, \pi/2)$ . Figure 2(c) shows that the total dispersive width in the insulating BSCCO is comparable to that in CCOC but is larger than that in undoped LSCO ( $\text{La}_2\text{CuO}_4$ ) by a factor of  $\sim 1.7$ . Here, it should be cautioned that spectra near  $(\pi, 0)$  of BSCCO may be influenced by possible bilayer splitting and that the intensity of the bonding band (BB) and antibonding band (AB) show different  $h\nu$ -dependence [25]. In order to check this possibility, we measured the photon energy dependence of the spectra of heavily underdoped samples ( $\delta \sim 0.025$  and  $0.06$ ) at  $(\pi, 0)$  from  $h\nu = 30$  eV to 60 eV with 5 eV photon energy interval, where the relative intensities of the BB and AB are expected different. We did not find appreciable photon-energy dependence in the line shape and the peak position from  $h\nu = 19$  eV. We therefore consider the impact of bilayer splitting on the  $(\pi, 0)$  electronic structure is small, partly because the  $(\pi, 0)$  state is already pushed considerably below the Fermi level.

In order to interpret the band dispersion in the parent insulator within the single-band description, we first con-

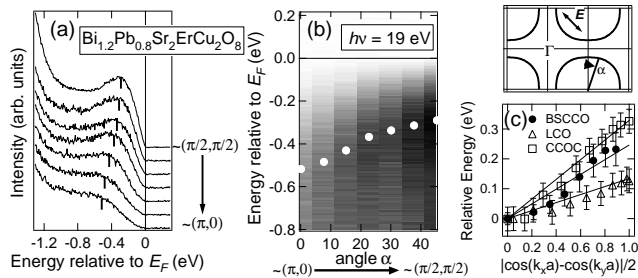


FIG. 2: ARPES spectra of  $\text{Bi}_{1.2}\text{Pb}_{0.8}\text{Sr}_2\text{ErCu}_2\text{O}_8$  along the “underlying Fermi surface” in the second BZ. (a) EDC’s. (b) Intensity plot in the  $E$ - $k$  plane. Vertical bars in (a) and the white circles in (b) indicate the points of maximum curvature in the EDC’s. (c) Peak positions referenced to the binding energy of the peak at  $(\pi/2, \pi/2)$  plotted against  $|\cos k_x a - \cos k_y a|/2$ . Also plotted are data for  $\text{La}_2\text{CuO}_4$  (LCO) and  $\text{Ca}_2\text{CuO}_2\text{Cl}_2$  (CCOC) [22].

consider the Hubbard ( $U$ - $t$ ) model or the  $t$ - $J$  model, where  $J = 4t^2/U$ , and  $t$ ,  $J$ , and  $U$  are the nearest neighbor hopping matrix element, the AF super-exchange coupling constant, and the on-site Coulomb energy, respectively. These models can explain the experimental band dispersion from  $(0,0)$  to  $(\pi,\pi)$  because its width is predicted to be  $\sim 2.2J$  ( $\sim 0.28$  eV) [23], however, they predict nearly the same peak energies for  $(\pi/2, \pi/2)$  and  $(\pi, 0)$ , disagreeing with the strong dispersion along the underlying Fermi surface in the insulating BSCCO. According to an extended version of the Hubbard model or the  $t$ - $J$  model, i.e., the  $t$ - $t'$ - $t''$ - $U$  model or the  $t$ - $t'$ - $t''$ - $J$  model, which takes into account the hopping to the second and third nearest neighbors through  $t'$  and  $t''$ , the strong dispersion from  $(\pi/2, \pi/2)$  to  $(\pi, 0)$  can be realized by a sizeable  $t'$  [11]. This implies a significantly larger value of  $|t'|$  in BSCCO than in LSCO.

In order to see further differences between BSCCO and LSCO, we show in Fig. 3 the ARPES spectra at  $(\pi, 0)$  (dashed curves) and AIPES spectra (solid curves) of BSCCO and LSCO. The AIPES spectra of LSCO have been obtained by integrating ARPES data within the second BZ. In the overdoped ( $\delta = 0.17$ ) BSCCO sample, one can see a well-known peak-dip-hump structure as observed in the ARPES spectra near the  $(\pi, 0)$  point [26, 27]. The intensity of the peak at  $\sim -40$  meV decreases with decreasing hole concentration or with increasing temperature (not shown). The dashed vertical bars in Fig. 3 mark the position of the flat band  $E(\pi, 0)$  (for BSCCO, BB and AB at higher and lower binding energies, respectively) in the ARPES spectra at  $(\pi, 0)$ . The solid vertical bars mark the point of the maximum curvature in the second derivatives of the AIPES spectra [12], also representing  $E(\pi, 0)$  in LSCO and the energy position of BB in BSCCO. In Fig. 4, those  $|E(\pi, 0)|$  values

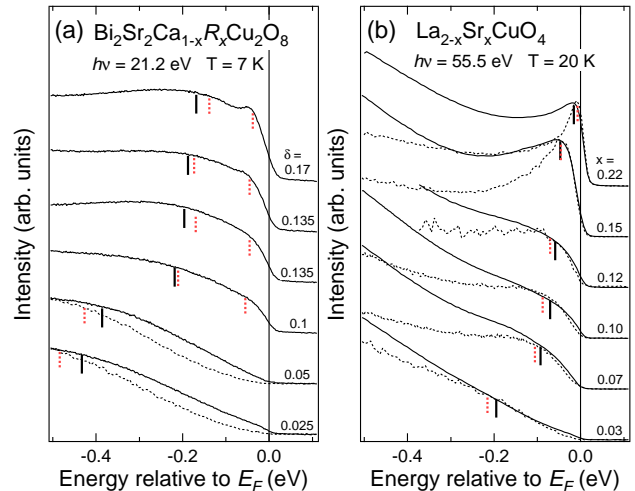


FIG. 3: AIPES spectra (solid curve) and ARPES spectra at  $(\pi, 0)$  (dashed curve) for various doping levels in BSCCO (a) and LSCO (b). Solid vertical bars indicate the point of maximum curvature and the dashed vertical bars mark the position of the flat band  $E(\pi, 0)$  (BB and AB at higher and lower binding energies, respectively, for BSCCO). ARPES data for BSCCO with  $\delta \geq 0.1$  was taken from [26, 27, 28]

for LSCO and BSCCO and the average energy positions of BB and AB for BSCCO,  $|E(\pi, 0)|$ , are plotted. One can see that  $|E(\pi, 0)|$  in BSCCO is larger by a factor of  $\sim 2$  than  $|E(\pi, 0)|$  in LSCO. Note that the magnitude of the small pseudogap, i.e., the binding energy of the leading edge position is also larger in BSCCO than in LSCO by a factor of  $\sim 2$  [14]. On the other hand, the  $J$  values are almost common between different families of cuprates [7, 8, 9, 10]. The present observation therefore suggests that the “band-structure” effect represented by  $t'$  has important effect on the magnitude of the large pseudogap. It should be noted that the energy position of the flat band was shown to become deeper with increasing  $|t'|$  according to the  $t$ - $t'$ - $t''$ - $J$  model calculations [11, 29]. As for the shape of the Fermi surface, since the flat band at  $(\pi, 0)$  especially of BB is deeper in BSCCO, the crossing point along the  $(0, 0)$ - $(\pi, \pi)$  line becomes closer to  $(0, 0)$  and that along the  $(\pi, 0)$ - $(\pi, \pi)$  line becomes closer to  $(\pi, \pi)$ , leading to the more “square-like” hole Fermi surface centered at  $(\pi, \pi)$  compared to the “diamond-like” hole Fermi surface in optimally-doped LSCO [29, 30]. Recently, the chemical potential shift as a function of doping was found to be faster in BSCCO than in LSCO [31], which can also be explained by a larger value of  $|t'|$  in BSCCO based on exact diagonalization studies of the  $t$ - $t'$ - $J$  model [32].

Figure 4 suggests that  $|E(\pi, 0)|$  of LSCO and  $|E(\pi, 0)|$  of BSCCO are scaled by  $T_{c, \max}$ . This implies possible relationship between  $T_{c, \max}$  and  $t'$ , as has been suggested in several different contexts [2, 5].  $T_{c, \max}$  in the high- $T_c$

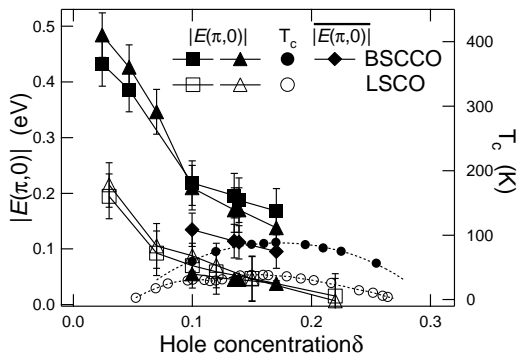


FIG. 4: Doping dependence of the flat band position  $E(\pi, 0)$  in BSCCO and LSCO determined by the second derivatives of AIPES spectra (squares) and ARPES spectra (triangles). The average energy position of BB and AB,  $|E(\pi, 0)|$ , for BSCCO (diamond) and  $T_c$  (circle) are also shown.

superconductors is determined by the block layer (and hence the position of the apical oxygen) as well as the number of  $\text{CuO}_2$  planes. It has been found from first-principles calculations that the values of  $t'$  and  $t''$  are different between different families of cuprates [5], while the other parameters are rather material-independent;  $U \sim 3$  eV,  $t \sim 0.3$  eV and  $J = 4t^2/U \sim 0.1$  eV. Therefore, it is quite natural to consider that the difference in  $t'$  (and probably  $t''$ ) rather than  $J$  strongly affects the  $T_{c,\text{max}}$ . Ohta *et al.* [1] argued that the Cu atom-apical oxygen distance affects the Madelung potential difference between the apical oxygen and the oxygen in the plane and thereby influences the stability of the Zhang-Rice singlet relative to the  $B_{1g}$  triplet where the hole enters the apical oxygen  $p_z$  orbital. According to Fleck *et al.* [4] and Tohyama *et al.* [33], the stability of charge stripes increases with decreasing  $|t'/t|$  but does not depend on  $J/t$ , consistent with the observation that LSCO is closer to the instability toward stripe-type spin-charge ordering [34]. It has also been proposed that the Fermi surface shape itself, which is influenced by  $t'$  and  $t''$ , is important to increase  $T_{c,\text{max}}$  [5]. More theoretical studies are needed to identify a microscopic mechanism in which larger  $|t'|$  leads to higher  $T_{c,\text{max}}$ .

In conclusion, we have identified several differences between the electronic structures of BSCCO and LSCO, all of which can be explained by the larger value of  $|t'|$  in BSCCO than in LSCO. In order to see whether there is indeed correlation between  $T_{c,\text{max}}$  and  $|t'|$ , further systematic studies on other materials (such as YBCO, Tl-bases cuprates, etc.) are highly desirable.

We acknowledge technical help by N. P. Armitage and K. M. Shen, and enlightening discussion with T. Tohyama, D. L. Feng, I. Dasgupta, E. Parvarini and O. K. Andersen. This work was supported by a Grant-in-Aid for Scientific Research in Priority Area “Novel Quantum

Phenomena in Transition-Metal Oxides” from the Ministry of Education, Culture, Sports, Science and Technology of Japan, the New Energy and Industrial Technology Development Organization (NEDO) and a US-Japan Joint Research Project from the Japan Society for the Promotion of Science. SSRL is operated by the DOE Office of Basic Energy Science Divisions of Chemical Sciences and Material Sciences. ALS is operated by the DOE Office of Basic Energy Science, Division of Material Science. This work was also performed under the approval of the Photon Factory Program Advisory Committee (Proposal No. 2002G174).

- 
- [1] Y. Ohta, T. Tohyama, and S. Maekawa, Phys. Rev. B **43**, 2968 (1991).
  - [2] R. Raimondi, J. H. Jefferson, and L.F. Feiner, Phys. Rev. B **53**, 8774 (1996).
  - [3] E. Dagotto, A. Nazarenko, A. Moreo, Phys. Rev. Lett. **74**, 310 (1995).
  - [4] M. Fleck, A.I. Lichtenstein, and A.M. Oleś, Phys. Rev. B **64**, 134528 (2001).
  - [5] E. Pavarini *et al.*, Phys. Rev. Lett. **87**, 047003 (2001).
  - [6] H. Eisaki *et al.*, *in press*.
  - [7] G. Blumberg *et al.*, Science **278**, 1427 (1997).
  - [8] S. Sugai, S. Shamoto, and M. Sato, Phys. Rev. B **38**, 6436 (1988).
  - [9] G. Blumberg *et al.*, Phys. Rev. B **53**, R11930 (1996).
  - [10] S.M. Hayden *et al.*, Physica B **241-243**, 765 (1998).
  - [11] C. Kim *et al.*, Phys. Rev. Lett. **80**, 4245(1998).
  - [12] A. Ino *et al.*, Phys. Rev. Lett. **81**, 2124 (1998).
  - [13] A. Ino *et al.*, J. Phys. Soc. Jpn **68**, 1496 (1999).
  - [14] A. Ino *et al.*, Phys. Rev. B **65**, 094504 (2002).
  - [15] X.J. Zhou *et al.*, Phys. Rev. Lett. **86**, 5578 (2001).
  - [16] T. Yoshida *et al.*, Phys. Rev. Lett. **91**, 027001 (2003).
  - [17] A. Ino *et al.*, Phys. Rev. Lett. **79**, 2101 (1997).
  - [18] T. Takemura *et al.*, J. Phys. Condens. Matter **12**, 6199 (2000).
  - [19] T. Kitajima *et al.*, J. Phys. Condens. Matter **11**, 3169 (1999).
  - [20] I. Terasaki *et al.*, Physica C **378**, 212 (2002).
  - [21] S.D. Obertelli, J.R. Cooper, and J.L. Tallon, Phys. Rev. B **46**, 14928 (1992).
  - [22] F. Ronning *et al.*, Science **282**, 2067 (1998).
  - [23] B.O. Wells *et al.*, Phys. Rev. Lett. **74**, 964 (1995).
  - [24] Z.-X. Shen *et al.*, Science **267**, 343 (1995). Note, however, that there is a systematic deviation (rounding off) from the  $d_{x^2-y^2}$ -like behaviour, i.e.,  $|\cos k_x a - \cos k_y a|/2 \sim 0$ , near  $(\pi/2, \pi/2)$ . The same deviation was also seen in CCOC [22].
  - [25] D.L. Feng *et al.*, Phys. Rev. Lett. **86**, 5550 (2001); A. A. Kordyuk *et al.*, Phys. Rev. Lett. **89**, 077003 (2002).
  - [26] D.S. Dessau *et al.*, Phys. Rev. Lett. **66**, 2160 (1991).
  - [27] D.L. Feng *et al.*, Science **289**, 277 (2000).
  - [28] J.C. Campuzano *et al.*, Phys. Rev. Lett. **83**, 3709 (1999).
  - [29] P. Prelovsek and A. Ramsak, Phys. Rev. B **65**, 174529 (2002).
  - [30] T. Tohyama and S. Maekawa, Supercond. Sci. Technol. **13**, R17 (2000).
  - [31] N. Harima *et al.*, Phys. Rev. B **67**, 172501 (2003).

- [32] T. Tohyama and S. Maekawa, Phys. Rev. B **67**, 092509 (2003).
- [33] T. Tohyama *et al.*, Phys. Rev. B **59**, 11649 (1999).
- [34] M.I. Salkola, V.J. Emery, and S.A. Kivelson, Phys. Rev. Lett. **77**, 155 (1996).